

Localization behavior of Dirac particles in disordered graphene superlattices

Qifang Zhao and Jiangbin Gong*

*Department of Physics and Centre for Computational Science and Engineering,
National University of Singapore, Singapore 117546, Republic of Singapore*

Cord A. Müller

Centre for Quantum Technologies, National University of Singapore, Singapore 117543, Republic of Singapore

Graphene superlattices (GSLs), formed by subjecting a monolayer graphene sheet to a periodic potential, can be used to engineer band structures and, from there, charge transport properties, but these are sensitive to the presence of disorder. The localization behavior of massless 2D Dirac particles induced by weak disorder is studied for both scalar-potential and vector-potential GSLs, computationally as well as analytically by a weak-disorder expansion. In particular, it is investigated how the Lyapunov exponent (inverse localization length) depends on the incidence angle to a 1D GSL. Delocalization resonances are found for both scalar and vector GSLs. The sharp angular dependence of the Lyapunov exponent may be exploited to realize disorder-induced filtering, as verified by full 2D numerical wave packet simulations.

PACS numbers: 72.80.Vp, 71.23.An, 73.20.Fz, 73.20.Jc, 73.21.Cd

I. INTRODUCTION

One fundamental aspect of graphene lies in the linear dispersion relation of its low-energy charge carriers (electrons and holes) around the so-called Dirac points. These charge carriers behave as relativistic massless chiral Dirac fermions and can be described by a two-dimensional (2D) Dirac equation.^{1–3} The linear dispersion relation is responsible for many discoveries in recent graphene research,⁴ such as half-integer quantum Hall effect,^{5,6} Klein’s paradox,^{7,8} and Zitterbewegung.⁹ Other than to graphene, Dirac or Dirac-like equations naturally apply to cold atoms,^{10–14} trapped ions,¹⁵ semiconductors,¹⁶ or polaritons.¹⁷

Motivated by the importance of Dirac equations in such a wide variety of frontier research areas, we study in this work disorder-induced localization^{18,19} of massless Dirac particles in random potentials. Though our results are presented in the context of disordered graphene superlattices (GSLs, see below) we expect them to be useful for many other settings as well. For example, when disorder is introduced to cold-atom simulations of graphene¹¹ or GSLs,¹⁴ our general treatment can be adapted to study the impact of randomness on the transport of Dirac matter waves.

GSL refers to graphene under external periodic scalar^{20–28} or vector potentials.^{28–36} Because GSLs further tailor the band dispersion relation of graphene, they may be used to construct graphene-based quantum devices. Theoretical studies of GSLs and graphene under periodic corrugation^{37–39} have been highly fruitful, with remarkable findings such as electron beam supercollimation²³ and the emergence of extra Dirac points.^{25–28} On the experimental side, GSLs with scalar potential barriers can be created via the electric field effect or chemical doping.^{40–42} Two-dimensional (2D) GSLs with a period as small as 5 nm have been created through electron-beam induced deposition of carbon.⁴³

Also triangular GSLs growing on different metal surfaces have been observed.^{44–50} Besides, nano-ripple arrays are generated by chemical vapor deposition (CVD).⁵¹ Vector potentials are induced by magnetic fields⁵² or physical strain,⁵³ so vector GSLs can be realized by mounting graphene on a substrate with a periodic array of ferromagnetic strips or a periodically structured substrate.⁵⁴

All these laboratory-produced GSLs cannot be perfectly periodic, due to intrinsic randomness and uncontrollable factors during production. Therefore, a more realistic GSL should be modeled by a periodic potential plus some weak disorder in potential height, potential width, or lattice spacing. This randomness causes Anderson localization, which turns conductors into insulators and is especially severe in low dimensions.^{18,19} Consequently, the focus of our work is on the localization behavior of a 2D Dirac particle in weakly disordered 1D GSLs. In a related work,⁵⁵ localization of Dirac particles in 1D disordered potentials was studied, but only for zero incidence angle θ (i.e., wave vector of charge carriers normal to the interface between different GSL layers) and without analytical results for the localization length. Another closely related theoretical study of disordered GSLs⁵⁶ comprised an analytical discussion of the scattering transmission only for sufficiently small θ and random barrier heights. Our work extends all previous results, to the best of our knowledge, inasmuch as it covers the analytical properties of the localization length for all values of θ , for different types of disorder, and for both scalar and vector GSLs.

The paper is organized as follows. In Sec. II, we begin by modeling disordered scalar and vector GSLs by 1D rectangular potential barriers or wells. Using a transfer matrix formalism, we then derive the weak-disorder expansion of the localization length, or equivalently the associated Lyapunov exponent. In Sec. III we present analytical and numerical results for the Lyapunov exponent of scalar GSLs, as modeled by disordered delta or

rectangular potentials. It is found that at fixed energy, the localization length depends very intricately upon the incidence angle θ of 2D Dirac particles in the graphene plane. We also predict and confirm the existence of delocalization resonances other than for perpendicular incidence: along these directions the Lyapunov exponent vanishes. Our theoretical predictions are fully supported by numerical results, as also reported below. Section IV is in parallel with Sec. III, but treats GSLs with vector potentials. In addition, assisted by a numerical study of wave-packet dynamics in Sec. V, we propose to use the angular dependence of the localization length to realize a disorder-based filtering mechanism. Section VI concludes.

II. LOCALIZATION LENGTH IN DISORDERED GRAPHENE SUPERLATTICES

A. Disordered graphene superlattices

Thanks to their linear dispersion relation, low-energy charge carriers near the Dirac points in graphene are well described by the 2D massless Dirac Hamiltonian:

$$H = v_F \boldsymbol{\sigma} \cdot \mathbf{p} + V(x). \quad (1)$$

In graphene, $v_F \approx 10^6$ m/s is the Fermi velocity; $\boldsymbol{\sigma} \equiv (\sigma_x, \sigma_y)$ is the vector of Pauli matrices. We consider a graphene superlattice (GSL) of parallel potential barriers, such that the external potential $V(x)$ depends only on x . In the following, we consider both scalar and vector superlattices.

A general scalar superlattice potential can be described by

$$V(x) = \sum_{n \in \mathbb{Z}} V_n(x - x_n). \quad (2)$$

We will consider rectangular potential barriers (or wells) as depicted in Fig. 1. A perfect GSL has identical potential barriers (or wells) of height V and width w , i.e. $V_n(x) = V$ if $0 < x < w$ and 0 elsewhere, at lattice positions $x_n = nl$. Due to unavoidable experimental imperfections, or deliberate introduction of randomness, these potential parameters fluctuate from site to site:

$$V_n = V + \delta V_n, \quad (3)$$

$$x_n = nl + \delta x_n, \quad (4)$$

$$w_n = w + \delta w_n. \quad (5)$$

This randomness can induce localization, as will be discussed at length in Sec. III.

A vector-potential superlattice is defined in terms of the matrix-valued potential

$$V(x) = -\sigma_y \frac{e v_F}{c} \sum_{n \in \mathbb{Z}} A_n(x - x_n). \quad (6)$$

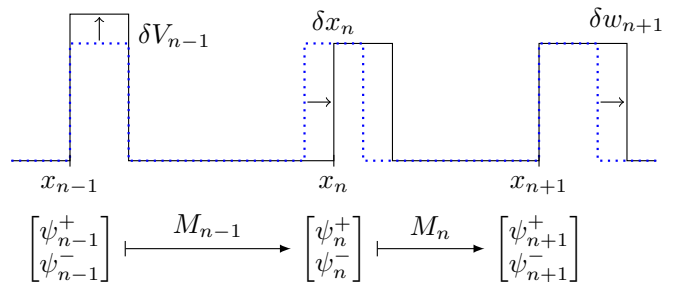


FIG. 1. Top: Disordered graphene superlattice (GSL) realized as a scalar potential, Eq. (2), or vector potential, Eq. (6). Deviations from the clean GSL (dotted) can occur via fluctuations in barrier height δV , barrier width δw , lattice spacing δl , and combinations thereof. Bottom: Right- and left-travelling wavefunction amplitudes are mapped from one barrier to the other by the transfer matrix, Eq. (11).

Defining $V_n = e v_F A_n / c$ and assuming $A_n(x - x_n)$ is of the same form as $V_n(x - x_n)$, one deals with the same parameters as in the scalar case. The different potential nature, however, implies very different localization properties, as will become clear in Sec. IV.

B. Transfer-matrix formalism

Because the potential $V(x)$ is separable, the problem of describing the transmission across the lattice is effectively 1D, and the transfer matrix formalism is particularly suited.⁵⁷

The scattering of a massless Dirac particle through a single square barrier (well) is well understood, for scalar as well as vector potentials.^{8,53} Since the potential is piecewise constant, the solution to the Dirac equation is a plane wave, both inside and outside the barrier. Outside the barrier, solutions of energy $E = s \hbar v_F k$ with $s = \pm 1$ and $k = |\mathbf{k}| = (k_x^2 + k_y^2)^{1/2}$ are the Dirac bispinors

$$\Psi^\pm(x, y) = e^{\pm i k_x x + i k_y y} \begin{pmatrix} 1 \\ \pm s e^{\pm i \theta} \end{pmatrix}, \quad (7)$$

travelling towards right (+) and left (-), with $k_x \geq 0$ by convention.

$$\theta = \tan^{-1} \frac{k_y}{k_x} \quad (8)$$

is the incidence angle, or angle of propagation (outside the barrier) with respect to the x -axis.

In the lattice, the wave function between barriers, where $V(x) = 0$, is a superposition of free right- and left-moving components created by repeated elastic reflection and transmission. It is useful to parametrize the wave function on the left side of the n th barrier, $\Psi_n = \lim_{\epsilon \rightarrow 0^+} \Psi(x_n - \epsilon)$, as

$$\Psi_n = \psi_n^+ \begin{pmatrix} 1 \\ s e^{i \theta} \end{pmatrix} e^{i k_y y} + \psi_n^- \begin{pmatrix} 1 \\ -s e^{-i \theta} \end{pmatrix} e^{i k_y y}. \quad (9)$$

Since the free solutions (7) between barriers are fixed, scattering cannot mix the two components of the bispinor, and it suffices to introduce the two amplitudes ψ_n^\pm , just as for a scalar wave obeying Schrödinger's equation on a 1D lattice. These amplitudes are mapped from n to $n+1$ by the transfer matrix:

$$\begin{bmatrix} \psi_{n+1}^+ \\ \psi_{n+1}^- \end{bmatrix} = M_n \begin{bmatrix} \psi_n^+ \\ \psi_n^- \end{bmatrix} \quad (10)$$

with

$$M_n = \begin{bmatrix} \frac{1}{t_n^*} e^{i\Delta_n} & -\frac{r_n^*}{t_n^*} e^{i\Delta_n} \\ -\frac{r_n}{t_n} e^{-i\Delta_n} & \frac{1}{t_n} e^{-i\Delta_n} \end{bmatrix}. \quad (11)$$

Reflection and transmission amplitudes r_n and t_n are known functions of barrier parameters $\{V_n, x_n, w_n\}$ and quantum numbers $\{k_x, k_y, s\}$ or equivalently $\{E, \theta, s\}$ ^{8,53}. $\Delta_n \equiv k_x(x_{n+1} - x_n)$ is the free propagation phase between superlattice points in the absence of any barriers. The transfer matrix is largely determined by the symmetries of the scattering problem.^{57,58} Unitarity or current conservation implies $\det M_n = 1 = |r_n|^2 + |t_n|^2$. Thus the total reflection and transmission probabilities can be expressed as $R_n = |r_n|^2 = \sin^2 \phi_n$ and $T_n = |t_n|^2 = \cos^2 \phi_n$, and we find it useful to parameterize M_n as

$$M_n = \begin{bmatrix} e^{i\alpha_n} \sec \phi_n & e^{i\beta_n} \tan \phi_n \\ e^{-i\beta_n} \tan \phi_n & e^{-i\alpha_n} \sec \phi_n \end{bmatrix}. \quad (12)$$

By construction, the net transfer matrix across N barriers is the product

$$P_N = \prod_{n=1}^N M_n. \quad (13)$$

Before studying this product for the random matrices M_n arising from disorder, we first discuss its implications for clean GSLs.

C. Clean graphene superlattices

In a clean GSL, all transfer matrices $M_n = M$ are identical. In other words, a single transfer matrix contains all information about the dispersion relation in the lattice, which is the essence of Bloch's theorem.

If parameters are such that $|\text{tr}M| < 2$, the energy E lies within the conduction band of the GSL. In this case the eigenvalues of the transfer matrix are of the form $\lambda_\pm = e^{\pm i\mu}$ with $\mu \in \mathbb{R}$, such that $\text{tr}M = 2 \cos \mu$. The transfer phase $\mu = K_x l$ across one lattice cell determines the Bloch vector K_x of the extended solution in the x direction. In terms of the parametrization Eq. (12) the dispersion relation in the clean GSL therefore reads^{26,57}

$$\cos K_x l = \cos \mu = \sec \phi \cos \alpha. \quad (14)$$

The structure of this dispersion is analogous to that of the Kronig-Penny model,⁵⁹ from which it differs only in the functional dependence of the transfer parameters $\{\phi, \alpha\}$ on the potential parameters $\{V, l, w\}$ and $\{E, \theta, s\}$. This dependence will be made explicit for the two cases of scalar and vector potentials in Secs. III and IV, respectively.

In the case $|\text{tr}M| > 2$, the energy E falls into a band gap. The wave cannot propagate, and $|\text{tr}M| = 2 \cosh \kappa_x l$ defines the exponential decay rate $\gamma = \kappa_x l$ across one lattice cell. This characteristic localization exponent

$$\gamma = \ln |\lambda_+| \quad (15)$$

is determined by the larger one of the two eigenvalues of the transfer matrix M , which also defines the Lyapunov exponent of the product $P_N = M^N$, whose larger eigenvalue grows like $\exp\{\gamma N\}$.

D. Disordered graphene superlattices

The transmission across a disordered lattice is described by the product P_N of random matrices shown in Eq. (13). Since the pioneering work of Furstenberg,⁶⁰ it is well known that the larger eigenvalue of such a product grows exponentially with probability one. This implies that a wave incident on the disordered GSL at barrier number 1 has an exponentially small probability of transmission after barrier number N , which is one of the hallmarks of disorder-induced localization. Indeed, at the first barrier, the wave splits into reflected and transmitted components, and so on across the lattice. The boundary condition is actually simpler after the last barrier N , where there is only the transmitted component, but no component is incident from the right. Starting with the reverse boundary condition (such as $\psi_1^+ = 1$ and $\psi_1^- = 0$) at the left, the product in Eq. (13) predicts that the solution grows like

$$|\psi_N^+|^2 = |(P_N)_{11}|^2 \sim \exp\{2N\gamma\}, \quad (16)$$

which suggests the expected exponential localization. The Lyapunov exponent, mathematically defined as

$$\gamma = \lim_{N \rightarrow \infty} \frac{1}{2N} \ln |(P_N)_{11}|^2 = - \lim_{N \rightarrow \infty} \frac{1}{2N} \ln T_N, \quad (17)$$

thus determines the localization length $l_{\text{loc}} = l/\gamma$. Here $T_N \in [0, 1]$ is the net transmission probability after N barriers.

The transmission is a random variable, with a very wide probability distribution for long enough samples. In the localized regime, its most probable (or typical) value differs vastly from its mean. The extinction $|\ln T(N)|$, however, has a probability distribution that converges towards a normal distribution, such that its most probable value is equal to the mean, and the right hand side of Eq. (17) indeed converges to the Lyapunov exponent.^{58,61}

While it is an elementary exercise to multiply random matrices and extract the Lyapunov exponent numerically, there is no simple, general method of calculating the Lyapunov exponent exactly for a given model of disorder with arbitrary energy. Different situations require different approaches. In the following, we treat two different cases that are relevant in the GSL context and allow for analytical calculations.

E. Randomly spaced, identical barriers

First we consider the very simple case where identical barriers are distributed with random positions such that the free propagation phase between barriers is uniformly distributed in $[0, 2\pi]$. Under an ensemble average $\overline{(\cdot)}$ over these random phases, the extinction $|\ln T_N|$ across N barriers is found to be additive along the sample: $\overline{|\ln T_N|} = N \ln T_1$.^{58,62} Here, T_1 is the single-barrier transmission at given energy E and propagation angle θ . Equation (17) then immediately yields the Lyapunov exponent $\gamma = -\frac{1}{2} \ln T_1$. This result holds as long as the phases are random enough to satisfy the assumption of a uniform distribution, but no matter how small T_1 , i.e. how strong the scattering.

At a given energy, a rectangular barrier becomes perfectly transmitting at certain incident angles, and notably at perpendicular incidence ($\theta = 0$) for all energies—this phenomenon is known as Klein tunneling.⁸ In these cases, $T_1 = 1$ implies of course $\gamma = 0$ and absence of localization, because all barriers share the same resonance condition.

F. Weak-disorder expansion

Although the previous elementary model captures the essence of disorder-induced exponential localization, it cannot describe the more interesting, and arguably more relevant, case of barriers with slightly random width, height, and/or spacing. In the following, we adapt the weak-disorder expansion of Derrida et al.⁶³ to our case. Here, we describe briefly the steps leading to the main result; details can be found in Appendices.

First, we Taylor-expand

$$M_n = M + \epsilon_n M' + \frac{\epsilon_n^2}{2} M'' + O(\epsilon_n^3), \quad (18)$$

where M is the transfer matrix of the corresponding clean GSL, the prime $(\cdot)'$ indicates differentiation with respect to the perturbed variable V , w or d , and ϵ_n is the weak perturbation ($\epsilon_n = \delta V_n$, δw_n or δd_n). We assume that the random variables at different sites are independent and identically distributed, with zero mean and finite

variance:

$$\bar{\epsilon} = \lim_{N \rightarrow \infty} \frac{1}{N} \sum_{n=1}^N \epsilon_n = 0, \quad (19)$$

$$\bar{\epsilon}^2 = \lim_{N \rightarrow \infty} \frac{1}{N} \sum_{n=1}^N \epsilon_n^2 \geq 0. \quad (20)$$

Second, we expand the product (13) to order ϵ^2 in the eigenbasis of M , where $\tilde{M} = \text{diag}(\lambda_+, \lambda_-)$. The eigenbasis of M can be used to find the Lyapunov exponent because the exponential growth rate is independent of the representation. The matrix element required in (16) then reads, neglecting terms of order ϵ^3 ,

$$(\tilde{P}_N)_{11} = \lambda_+^N \left[1 + \lambda_+^{-1} \sum_{n=1}^N \left\{ \epsilon_n \tilde{M}'_{11} + \frac{\epsilon_n^2}{2} \tilde{M}''_{11} \right\} + \sum_{n < m} \epsilon_n \epsilon_m \lambda_+^{n-m-1} (\tilde{M}' \tilde{M}^{m-n-1} \tilde{M}')_{11} \right]. \quad (21)$$

The second line involves only fluctuations at different sites and gives no contribution after the ensemble average (see App. A1 for details). Inserting the first line into Eq. (17), and further using Eqs. (19) and (20), one obtains the disorder-induced Lyapunov exponent

$$\gamma = \frac{l}{l_{\text{loc}}} = \frac{\bar{\epsilon}^2}{2} \text{Re} \left\{ \lambda_+^{-1} \tilde{M}''_{11} - \lambda_+^{-2} \left(\tilde{M}'_{11} \right)^2 \right\}. \quad (22)$$

In a third step we perform the diagonalization from M to \tilde{M} in order to arrive at an explicit expression as function of the system variables (see App. A2 for details). In terms of the parametrization (12) one obtains a relatively compact result:

$$\gamma = \frac{\bar{\epsilon}^2}{2} \left\{ \frac{\tan^4 \phi}{\sin^2 \mu} \left[\left(\frac{\sin \alpha}{\sin \phi} \right)' \right]^2 + \beta'^2 \tan^2 \phi \right\}. \quad (23)$$

Here, $\sin \mu$ is a function of $\{\alpha, \phi\}$ via the clean dispersion relation (14), which is assumed to be satisfied by a propagating solution of energy E (otherwise, this perturbative result of order $\bar{\epsilon}^2$ is merely a small correction to the band-gap extinction of Sec. IID).

Before we discuss the localization exponent (23) in detail for scalar and vector potentials (Secs. III and IV), we comment on its limit of validity. Eq. (23) diverges at the band edges, where $\sin \mu = 0$. It is well known that localization at these special points occurs with an anomalous localization length that differs from the perturbative result.^{64,65} However, exponential localization in the conduction band away from these special points is very well described by Eqs. (22) and (23), as will be checked via numerical calculations below.

III. SCALAR POTENTIAL

Now we specify the transfer-matrix parametrization in Eq. (12) for a single scalar potential barrier, the building

block of the scalar GSL, in order to analyze the Lyapunov exponent given in Eq. (23). The reflection and transmission amplitudes r and t are found by piecing together a continuous plane-wave solution across the barrier:⁸

$$\frac{1}{t} = e^{i w k_x} \left[\cos \varphi + i s \sin \varphi \frac{v - \varepsilon \cos^2 \theta}{q l \cos \theta} \right], \quad (24)$$

$$\frac{r}{t} = -s e^{i w k_x} e^{i \theta} \tan \theta \frac{v \sin \varphi}{q l}. \quad (25)$$

Here $\varepsilon = E l / \hbar v_F = s |\mathbf{k}| l$ and $v = V l / \hbar v_F$ are energy and barrier height expressed in lattice units. Furthermore, $\varphi = q w$ is the phase picked up by the plane wave with wavevector $q = [(v - \varepsilon)^2 l^{-2} - k_y^2]^{1/2}$ in the x -direction across the potential barrier.

In the next Sec. III A, we first discuss the limiting case of δ -like barriers, which admits simple expressions and helps to guide the understanding of the general case, tackled in Sec. III B.

A. Amplitude-disordered delta scalar potential

Consider an amplitude-disordered Dirac-Kronig-Penney model, made out of regularly spaced δ -peaks of random strength, or δ GSL for short. This description is appropriate in the low-energy regime, where barriers become very narrow and high, $k_x w \ll 1$ and $v \gg \varepsilon$. In the limit $w \rightarrow 0$ and $v \rightarrow \infty$ at fixed $v w / l = \varphi$, one has $q l \rightarrow v$, and the reflection and transmission coefficients in Eqs. (24) and (25) become

$$\frac{1}{t} = \cos \varphi + i s \frac{\sin \varphi}{\cos \theta}, \quad (26)$$

$$\frac{r}{t} = -s e^{i \theta} \tan \theta \sin \varphi. \quad (27)$$

These expressions depend on the barrier parameters only via the combination $\varphi = v w / l$. Therefore, they cover randomness in both barrier width and height. We assume a resulting phase-shift distribution with mean $\overline{\varphi} = \overline{\varphi}_n$, and fluctuations $\epsilon_n = \varphi_n - \varphi$ with variance $\overline{\epsilon^2} = \overline{\delta \varphi^2}$.

Substituting Eqs. (26) and (27) into Eq. (11) and then comparing with Eq. (12), one has

$$e^{i \alpha} \sec \phi = \left(\cos \varphi - i s \frac{\sin \varphi}{\cos \theta} \right) e^{i k_x l}, \quad (28)$$

$$e^{i \beta} \tan \phi = s \sin \varphi \tan \theta e^{-i \theta} e^{i k_x l}. \quad (29)$$

Taking the real part of the first relation, we find the clean dispersion for this δ GSL,

$$\cos \mu = \cos k_x l \cos \varphi + \frac{\varepsilon}{k_x l} \sin k_x l \sin \varphi. \quad (30)$$

We recall $k_x l = [\varepsilon^2 - l^2 k_y^2]^{1/2} = s \varepsilon \cos \theta$. This relation links the energy ε to the Bloch-vector components $K_x = \mu / l$ and $K_y = k_y$ in the bulk superlattice. The dispersion is periodic in the potential strength φ , as discussed in detail by Barbier et al.⁶⁶, and it suffices to consider $0 \leq \varphi < 2\pi$. In the following, the implications of disorder are assessed.

1. Analytical Lyapunov exponent

From Eq. (29), it becomes apparent that $\beta = k_x l - \theta$ is independent of φ . Consequently, $\beta' = 0$ in Eq. (23). Furthermore, by combining both relations, we can evaluate $\partial_\varphi(\sin \alpha / \sin \phi)$ such that the weak-disorder Lyapunov exponent finally reads

$$\gamma = \frac{\overline{\delta \varphi^2}}{2} \frac{\sin^2 k_x l}{\sin^2 \mu} \tan^2 \theta. \quad (31)$$

This expression differs in a characteristic manner from the corresponding result for a massive Schrödinger particle:⁶⁸ instead of being inversely proportional to the energy, it is proportional to $\tan^2 \theta$. This has (at least) three important implications: First, instead of diverging as ε^{-1} , the weak-disorder result of Eq. (31) stays valid even at low energy ε . Second, for perpendicular incidence $\theta = 0$, there is no localization, $\gamma = 0$, as required by chiral symmetry via Klein tunneling^{8,55}. Third, the overall angular dependence as $\tan^2 \theta$ implies that charge carriers incident with larger angles are localized quite rapidly. Therefore, a random δ GSL can act as a *directional filter*, with preferential transmission perpendicular to the superlattice barriers.

Indeed, in the case $\varphi = 0$, i.e., for a purely random potential without a regular superlattice component, Eq. (30) reduces to $\mu = k_x l$, and the Lyapunov exponent

$$\gamma = \frac{\overline{\delta \varphi^2}}{2} \tan^2 \theta \quad (32)$$

becomes totally independent of energy ε . The simple, and sharp angular dependence $\tan^2 \theta$ realizes a disorder filter at larger angles, allowing only particles around perpendicular incidence $\theta = 0$ to transmit ballistically.

Of course, a richer angular structure arises via the dependence on $k_x l = s \varepsilon \cos \theta$ and the dispersion relation in Eq. (30), so that a more detailed discussion is in order. It is helpful to distinguish two limiting cases. First, for $\varepsilon \rightarrow 0$ and thus $k_x l \rightarrow 0$, Eq. (30) always has the real (hence propagating) solution $\mu = K_x l = \varphi$. Therefore, unless $\varphi = 0, \pi$, one has $\sin k_x l / \sin \mu \rightarrow 0$, and therefore delocalization ($\gamma \rightarrow 0$) occurs for all angles as $\varepsilon \rightarrow 0$. Second, for large enough $|\varepsilon| \geq \pi$, one has $\sin k_x l = 0$ for $\varepsilon \cos \theta_n = n\pi$ ($n \neq 0$), while allowing $\cos \mu = \pm \cos \varphi \neq 0$. Equation (31) then indicates that $\sin k_x l = 0$ gives angular transmission windows $\gamma = 0$ at

$$\theta_n = \arccos(n\pi/\varepsilon). \quad (33)$$

Therefore, if the incident angle of a 2D plane wave is θ_n , then the Dirac particle will be delocalized.

2. Numerical experiment

We now turn to numerical experiments in order to check these predictions. The localization Lyapunov exponents are extracted numerically by use of Eq. (17), after

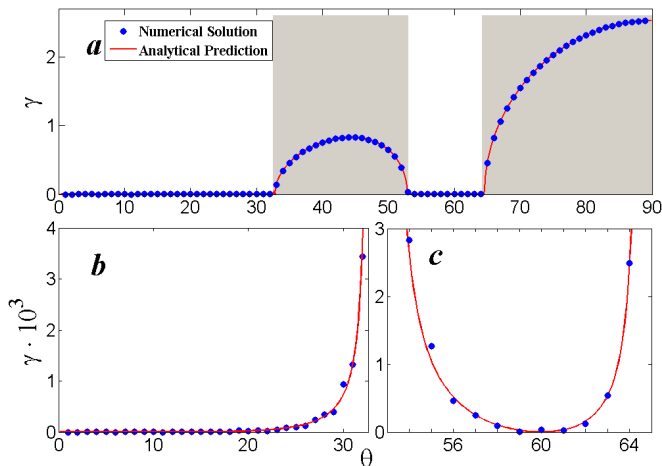


FIG. 2. Lyapunov exponent γ , Eq. (17), vs. angle θ at energy $\varepsilon = El/\hbar v_F = 2\pi$ in a lattice of δ -barriers with $\pm 5\%$ fluctuations around the average strength $\varphi = \pi/2$. In the grey shaded areas in panel **a**, the angle falls into a band-gap sector, and γ is given by Eq. (15). White areas: conduction sectors, with γ due to disorder given by Eq. (31), shown on a magnified scale in panels **b**, **c**. The numerical data confirms the delocalization resonance at $\theta_1 = \arccos(\pi/\varepsilon) = 60^\circ$, Eq. (33).

first multiplying random matrices according to Eq. (13). Unless specified otherwise, we always take $N = 1000$ random potential barriers and then ensemble-average over 30 samples to reach negligible statistical error.

Figure 2 compares the analytical result of Eq. (31) with the numerical data, for a varying incident angle θ at fixed energy $\varepsilon = 2\pi$. The average lattice strength is set to $\varphi = \pi/2$, and we allow 5% equiprobable fluctuations ($\overline{\delta v^2}/v^2 = 0.01/12$). In the overview panel **a**, grey shading shows the intervals where ε falls into a band gap. The incident wave then turns into an evanescent wave, whose attenuation is described by γ of Eq. (15), with negligible corrections due to disorder. For the given parameters, the band edges are located at angles θ_b solving $\cos \theta_b = \pm \sin(\varepsilon \cos \theta_b)$, i.e. $\theta_b \in \{32.7^\circ, 52.9^\circ, 64.6^\circ\}$. At these points, Fig. 2 shows hardly visible spikes, where the perturbative result of Eq. (31) is expected to fail.^{64,65} Inside the conduction intervals, shown in the magnified view of panels **b** and **c**, the Lyapunov exponent γ given by Eq. (31) is in excellent agreement with numerical results. The delocalization resonance at $\theta_1 = 60^\circ$ is confirmed, with γ vanishing there.

3. Exact delocalization resonance

Interestingly, the numerical evidence suggests that the delocalization resonance not only holds perturbatively to order ε^2 , as predicted by Eq. (31), but instead is an exact resonance. So we seek non-perturbative insights by returning to the transfer matrices. Under the resonance condition, $k_x l = \varepsilon \cos \theta_n = n\pi$, the free propagation phase is $e^{ik_x l} = \pm 1$. Without losing generality, let us

assume $e^{ik_x l} = 1$. The transfer matrix M_n in Eq. (12) then depends on the random variable φ_n via

$$M_n = M(\varphi_n) = \begin{bmatrix} \cos \varphi_n - i s \frac{\sin \varphi_n}{\cos \theta} & s \sin \varphi_n \tan \theta e^{-i\theta} \\ s \sin \varphi_n \tan \theta e^{i\theta} & \cos \varphi_n + i s \frac{\sin \varphi_n}{\cos \theta} \end{bmatrix}. \quad (34)$$

The product of transfer matrices obeys the remarkable property

$$M(\varphi_n)M(\varphi_{n-1}) = M(\varphi_n + \varphi_{n-1}). \quad (35)$$

Hence, the net transfer matrix across N barriers is $P_N = M(\Phi_N)$ where $\Phi_N = \sum_{n=1}^N \varphi_n$. As a consequence, the transmission probability

$$T_N = \frac{1}{\cos^2 \Phi_N + \frac{\sin^2 \Phi_N}{\cos^2 \theta}} = \frac{\cos^2 \theta}{1 - \sin^2 \theta \cos^2 \Phi_N}. \quad (36)$$

is bounded from below by $\cos^2 \theta$. So for the resonance angles θ_n of Eq. (33), T_N cannot be an exponentially decaying function of N , thus proving $\gamma = 0$. We emphasize that this delocalization is no longer based on a weak-disorder expansion. Rather, it is an exact result for arbitrary disorder strength.

B. Disordered square scalar potential

We return to the general case of a rectangular potential superlattice, and proceed as previously. With Eqs. (24) and (25) used in (11), the comparison with Eq. (12) yields

$$e^{i\alpha} \sec \phi = e^{i\delta} \left(\cos \varphi - i \sin \varphi \frac{\varepsilon v - \kappa^2}{\kappa q l} \right), \quad (37)$$

$$e^{i\beta} \tan \phi = e^{i(\delta-\theta)} \tan \theta \frac{v \sin \varphi}{s q l}. \quad (38)$$

We denote $\kappa = l k_x = s \varepsilon \cos \theta$ and $q l = [v^2 - 2\varepsilon v + \kappa^2]^{1/2}$, as well as $\varphi = q w$. We have introduced $\delta = k_x d$ as the phase picked up over the distance $d = l - w$ between barriers on average. In terms of these parameters, the dispersion relation of the clean GSL reads²⁶

$$\cos \mu = \cos \delta \cos \varphi + \frac{\varepsilon v - \kappa^2}{\kappa q l} \sin \delta \sin \varphi. \quad (39)$$

1. Lyapunov exponent

In the disordered case, Eq. (38) fixes $\beta = k_x d - \theta$, which now depends on the distance $d = l - w$ between consecutive barriers, such that β' in Eq. (23) is finite for barriers of variable distance d . By combining Eqs. (37) and (38), one finds

$$\gamma = \frac{\overline{\varepsilon^2}}{2} \left\{ \frac{v^2 \sin^2 \varphi}{q^2 l^2 \sin^2 \mu} [S\gamma]^2 + \beta'^2 \right\} \frac{v^2 \sin^2 \varphi}{q^2 l^2} \tan^2 \theta, \quad (40)$$

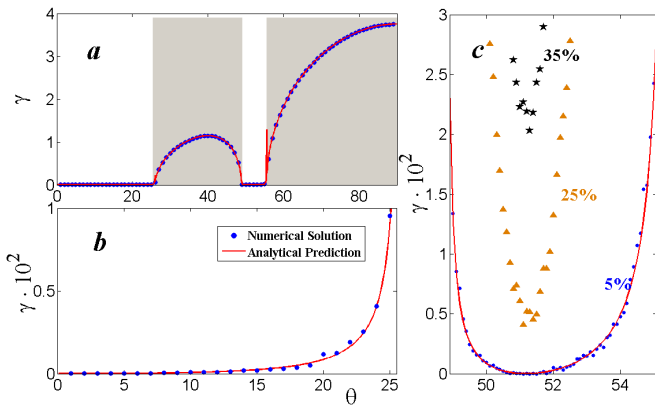


FIG. 3. Lyapunov exponent γ , Eq. (17), vs. angle θ at energy $\varepsilon = El/\hbar v_F = 2\pi$ in a lattice of potential barriers with fixed width $w = 0.5l$, and 5% fluctuations around average height $v = Vl/\hbar v_F = \pi$, such that $wv/l = \pi/2$ matches the δ barrier strength φ used in Fig. 2. In the grey shaded areas in panel **a**, the angle points into a band-gap direction, and γ is given by Eq. (15). White areas: conduction sectors, with γ due to disorder given by Eq. (40), shown on a magnified scale in panels **b**, **c**. The numerical data for stronger disorder in panel **c** shows that the perturbative delocalization resonance at $\theta \approx 51.5^\circ$ exists only for weak disorder.

where S' denotes the derivative of

$$S = \frac{ql \sin \delta \cos \varphi + k_x l \cos \delta \sin \varphi}{v \sin \varphi} - \frac{\varepsilon}{k_x l} \cos \delta \quad (41)$$

with respect to the fluctuating barrier parameter.

The relation between the Lyapunov exponent γ and the incidence angle θ established by Eqs. (40) and (41) is rather complicated. But the overall factor $\tan^2 \theta$ guarantees absence of localization due to Klein tunneling in the forward direction, as well as the efficient filtering of large-angle components. To verify our analytical prediction, we plot in Fig. 3 the Lyapunov exponent γ as function of θ at fixed ε for barriers with randomly varying height, together with the data from the numerical solution. The agreement is excellent.

2. Approximate delocalization resonance

The numerical results show that there exists a delocalization resonance $\gamma = 0$ also in this case, but at a slightly different angle, $\theta \approx 51.5^\circ$, compared to the δ -barriers of Sec. III A. Let us see how this result comes about. With $\beta' = 0$ (because in Fig. 3 only the barrier height fluctuates) in Eq. (40), there are two non-trivial factors that can vanish, $\sin \varphi$ and S' .

First, there is the obvious candidate $\sin \varphi = 0$, which is the single-barrier resonance condition $qw = n\pi$.⁸ But this zero is exactly cancelled by the most singular contribution to S' in Eq. (41), namely $S' = q\varphi' \sin \delta / (v \sin^2 \varphi) + O[(\sin \varphi)^{-1}]$. Since for $\sin \varphi = 0$ the dispersion relation Eq. (39) reads $\cos \mu = \pm \cos \delta$, Eq. (40) can be further

reduced to

$$\gamma = \frac{\overline{\delta v^2}}{2} \frac{w^2 v^2 (v - \varepsilon)^2}{l^6 q^4} \tan^2 \theta. \quad (42)$$

This expression could be thought to vanish for $v = \varepsilon$, i.e., when the energy equals the mean potential height. However, $v = \varepsilon$ implies $q = ik_y$, which is impossible because it contradicts the initially assumed resonance condition $qw = n\pi$.

Therefore, $S' = 0$ must be responsible for the observed delocalization resonance $\gamma = 0$. In general, the equation $S' = 0$ is too complicated to admit an analytical solution, but the resonance angles θ_n can be found numerically. For the present parameters it is the resonance angle θ_1 that is observed in Fig. 3. In contrast to the case of δ -barriers, though, this resonance is not exact. In Fig. 3c, numerical results for stronger disorder show a deviation from $\gamma = 0$, thus indicating the absence of a true delocalization resonance.

We note that for a purely random potential, $v = 0$ and $\varepsilon_n = v_n$, the Lyapunov exponent Eq. (40) reduces to

$$\gamma = \frac{\overline{\delta v^2}}{2} \frac{\sin^2(k_x w)}{k_x^2 l^2} \tan^2 \theta, \quad (43)$$

Now the single-barrier resonance condition $k_x w = n\pi$ does lead to $\gamma = 0$. Consistently, the limit $v \rightarrow 0$ of Eq. (42) vanishes. Here, to lowest order in $\varepsilon = \delta v$, the wavevector inside the barrier is k_x , and the resonance condition can be satisfied everywhere. But it needs to be emphasized that also this result holds only for weak disorder, and hence the Lyapunov exponent is not absolutely zero due to higher-order terms of ε .

IV. VECTOR POTENTIAL

This section parallels the previous one, with results pertaining to disordered vector-potential GSLs, as introduced in Eq. (6). The single-barrier reflection and transmission amplitudes r and t are⁵³

$$\frac{1}{t} = e^{i w k_x} \left(\cos \varphi - i \sin \varphi \frac{u \sin \theta + \varepsilon \cos^2 \theta}{\tilde{q} l \cos \theta} \right), \quad (44)$$

$$\frac{r}{t} = e^{i w k_x} e^{i \theta} \sec \theta \frac{u \sin \varphi}{\tilde{q} l}. \quad (45)$$

Here $\varepsilon = El/\hbar v_F = s|\mathbf{k}|l$ and $u = eAl/\hbar c$ are energy and barrier height expressed in lattice units. Besides, $\varphi = \tilde{q}w$ is the phase picked up by the plane wave with wavevector $\tilde{q} = l^{-1}[\varepsilon^2 - (lk_y - u)^2]^{1/2}$ across the potential barrier. The variable \tilde{q} differs from the wavevector q in the previous scalar potential case. In particular, \tilde{q} can be imaginary if u is large, leading to bound states inside a barrier.⁵³

A. Amplitude-disordered delta vector potential

Very narrow and high potentials barriers *i.e.*, $k_x w \ll 1$ and $u \gg \varepsilon$, realize a vector δ GSL. In the limit $w \rightarrow 0$ and $u \rightarrow \infty$ at fixed $uw/l = \varphi$, one has $\tilde{q} \rightarrow iu/l$, and the reflection and transmission coefficients in Eqs. (44) and (45) reduce to

$$\frac{1}{t} = \cosh \varphi - i \sinh \varphi \tan \theta, \quad (46)$$

$$\frac{r}{t} = e^{i\theta} \sec \theta \sinh \varphi. \quad (47)$$

The fluctuating phase $\varphi = uw/l$ describes randomness in both width w and height u . We assume a distribution with mean $\varphi = \overline{\varphi_n}$, and small fluctuations $\varepsilon_n = \varphi_n - \varphi$ with variance $\overline{\varepsilon^2} = \overline{\delta\varphi^2}$.

Substituting Eqs. (46) and (47) into Eq. (11) and comparing with Eq. (12), one has

$$e^{i\alpha} \sec \phi = (\cosh \varphi + i \sinh \varphi \tan \theta) e^{ik_x l}, \quad (48)$$

$$e^{i\beta} \tan \phi = -\sinh \varphi \sec \theta e^{-i\theta} e^{ik_x l}. \quad (49)$$

The clean dispersion (14) for the vector δ GSL is found by taking the real part of the first relation:

$$\cos \mu = \cosh \varphi \cos \kappa - \tan \theta \sinh \varphi \sin \kappa. \quad (50)$$

where $\kappa = k_x l = [\varepsilon^2 - l^2 k_y^2]^{1/2}$.

1. Lyapunov exponent

For regularly spaced potentials, $\beta' = 0$ in Eq. (23). Using Eqs. (48) and (49) to evaluate $\partial_\varphi(\sin \alpha / \sin \phi)$, we find the weak-disorder Lyapunov exponent

$$\gamma = \frac{\overline{\delta\varphi^2}}{2} \frac{\sin^2 k_x l}{\sin^2 \mu} \sec^2 \theta. \quad (51)$$

This expression resembles much the scalar δ GSL result (31), except that the $\tan^2 \theta$ factor is replaced by $\sec^2 \theta$. Therefore, vector δ GSL and scalar δ GSL share (at least) one interesting feature: Instead of diverging as ε^{-1} in the Schrödinger case, the weak-disorder prediction of the localization length stays valid even at low energy ε . On the other hand, because $\sec^2 \theta = 1$ at $\theta = 0$, there is no reason to expect delocalized solutions close to perpendicular incidence on general grounds.

2. Absence of delocalization resonances

For $\varphi = 0$, representing a random vector potential with zero mean, Eq. (51) reduces to the energy-independent expression $\gamma = \frac{1}{2} \overline{\delta\varphi^2} \sec^2 \theta$. The angular dependence $\sec^2 \theta$ differs from Eq. (32) for scalar δ GSL in that localization stays finite even at perpendicular incidence $\theta = 0$,

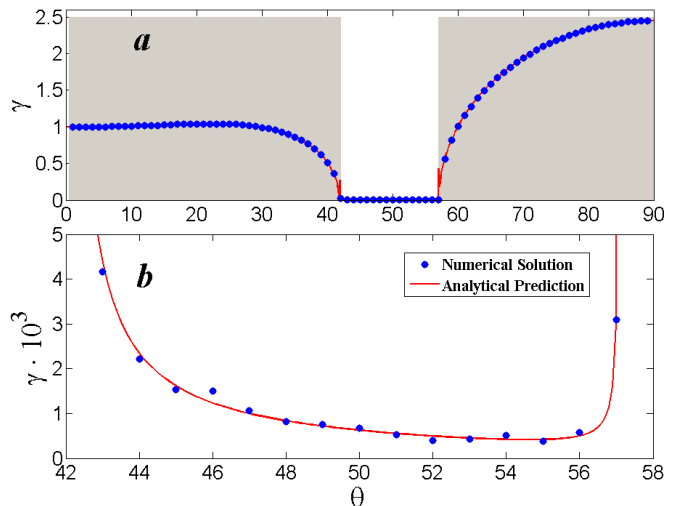


FIG. 4. Lyapunov exponent γ , Eq. (17), vs. incident angle θ , for a vector δ GSL, with average lattice strength $\varphi = 1$, energy $\varepsilon = 2\pi$, and disorder modeled by $\pm 5\%$ fluctuations around φ . In the grey shaded areas in panel **a**, the incident angle falls into a band-gap direction. The white area is the conduction sector, in which the analytical Lyapunov exponent is given by Eq. (51), as shown in Panel **b** on a larger scale.

but becomes just as strong at grazing incidence $\theta \rightarrow \pi/2$ where $\sec \theta \approx \tan \theta$.

For the general situation with $\varphi \neq 0$, we analyze two representative cases. Consider first the low-energy limit $\varepsilon \rightarrow 0$ and thus $\kappa \rightarrow 0$. Then the dispersion Eq. (50) reads $\cos \mu = \cosh \varphi$, which requires an imaginary μ and hence describes a non-propagating solution inside the band gap. As such, the vector δ GSL acts as an insulator for small ε and arbitrary incidence angle θ .

Next we turn to cases with sufficiently large $|\varepsilon| \geq \pi$. If $\varepsilon \cos \theta_n = n\pi$ ($n \neq 0$), one has $\sin \kappa = 0$ and hence $\gamma = 0$. Note that under this condition, $|\cos \mu| = \cosh \varphi$, which again implies a non-propagating solution. So here $\gamma = 0$ merely indicates that the disorder-induced correction to the decay exponent of the evanescent wave is zero. Putting all the above considerations together, it appears that the localization behavior in vector δ GSLs is not as rich as in scalar δ GSLs.

Figure 4 compares the analytical prediction Eq. (51) with numerical results, for varying incidence angle θ at fixed energy $\varepsilon = 2\pi$. The average lattice strength is $\varphi = 1$, and disorder is modeled by 5% equiprobable fluctuations around φ . In the overview panel **a**, band-gap regimes are grey shaded. The band edges lie at the angles $\theta_b \in \{42^\circ, 57^\circ\}$. Exactly at these points, abnormal spikes are seen in panel **a**, signaling the expected failure of Eq. (51).^{64,65} Inside the conduction band, shown on a magnified scale in panel **b**, the agreement between theory and numerics is excellent. In particular, no delocalization resonance is seen, as analyzed above.

B. Disordered square vector potential

The general case of a disordered rectangular vector potential is somewhat more complicated and considerably richer in physics. Following the same procedure as for scalar GSLs, the first step is to connect the transfer-matrix parameters α , β and ϕ to the GSL parameters w , u , and l , as well as the Dirac-particle quantum numbers ε , θ , s . For that purpose we use Eqs. (44), (45), (11), and (12) to obtain

$$e^{i\alpha} \sec \phi = e^{i\delta} \left(\cos \varphi + i \sin \varphi \frac{\kappa^2 + u\varepsilon \sin \theta}{l\tilde{q}\kappa} \right), \quad (52)$$

$$e^{i\beta} \tan \phi = -e^{i(\delta-\theta)} \frac{u \sin \varphi}{l\tilde{q}} \sec \theta. \quad (53)$$

Here $\kappa = lk_x = \varepsilon \cos \theta$, $l\tilde{q} = [\varepsilon^2 - (lk_y - u)^2]^{1/2}$, and $\varphi = \tilde{q}w$. $\delta = k_x(l - w)$ is the phase picked up between neighboring barriers. In terms of these parameters, the dispersion relation of a clean GSL becomes

$$\cos \mu = \cos \delta \cos \varphi - \frac{\kappa^2 + u\varepsilon \sin \theta}{l\tilde{q}\kappa} \sin \delta \sin \varphi. \quad (54)$$

1. Lyapunov exponent

Using Eqs. (52) and (53), we can apply our general result Eq. (23) once again, leading to

$$\gamma = \frac{\bar{\varepsilon}^2}{2} \left\{ \frac{u^2 \sin^2 \varphi}{l^2 \tilde{q}^2 \sin^2 \mu} [\tilde{S}'^2 + \beta'^2] \right\} \frac{u^2 \sin^2 \varphi}{l^2 \tilde{q}^2} \sec^2 \theta, \quad (55)$$

where \tilde{S}' denotes the derivative of

$$\tilde{S} = \frac{l\tilde{q} \sin \delta \cos \varphi + \kappa \cos \delta \sin \varphi}{u \sin \varphi} + \frac{\varepsilon}{\kappa} \cos \delta \sin \theta \quad (56)$$

with respect to the fluctuating barrier parameter. In contrast to the scalar potential with overall $\tan^2 \theta$ dependence, the factor $\sec^2 \theta$ in Eq. (55) does not lead to a simple delocalization resonance at perpendicular incidence, just as for the vector δ GSL of Sec. IV A.

Our numerical data confirm these predictions, as seen in Fig. 5. The statistical fluctuations in Fig. 5b appear larger than before because for the present parameters, the Lyapunov exponent γ is extremely small.

2. Approximate delocalization resonance

Figure 5 also reveals a delocalization resonance $\gamma = 0$ at $\theta \approx 18.5^\circ$, all the more remarkable because no such resonance occurs in the δ -barrier limit of Sec. IV A. In order to explain this analytically, we return to Eq. (55). First of all, for the amplitude randomness studied in Fig. 5, $\beta' = 0$. Then, $\gamma = 0$ at $u \neq 0$ implies $\sin \varphi = 0$ or $S' = 0$.

Let us begin by analyzing the case $\sin \varphi = 0$, which is equivalent to the barrier resonance condition $\tilde{q}w =$

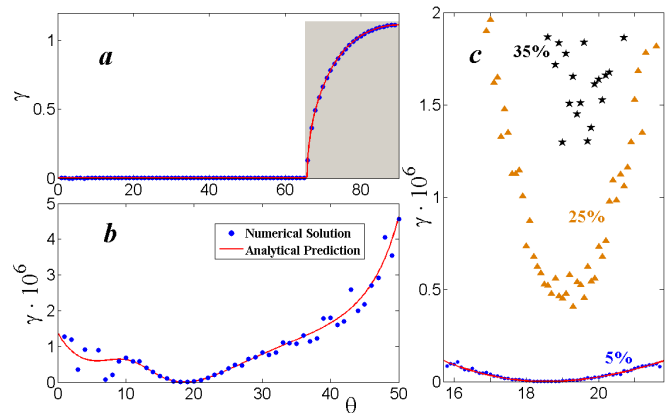


FIG. 5. Lyapunov exponent γ , Eq. (17), vs. incident angle θ , at energy $\varepsilon = 2\pi$ for a disordered lattice of rectangular vector potentials. Disorder is modeled by $\pm 5\%$ fluctuations around an average barrier height $u = 2$, while periodicity l and barrier width $w = 0.5l$ are fixed, such that $wu/l = 1$ matches the δ barrier strength φ used in Fig. 4. The grey shaded area in panel **a** indicates a band gap and the white area indicates conducting solutions. Panels **b** and **c** show details of the conduction sector. An approximate delocalization resonance appears around $\theta = 18.5^\circ$, for both analytical and numerical results. The numerical data for stronger disorder in Panel **c** proves the departure from the weak-disorder resonance.

$(w/l)[\varepsilon^2 - (\varepsilon \sin \theta - u)^2]^{1/2} = n\pi$. To leading order in $1/\sin \varphi$, we find $|S'| = |q\varphi' \sin \delta / (u \sin^2 \varphi)|$ from Eq. (56). So the $\sin^4 \varphi$ factors cancel in Eq. (55), which reduces to

$$\gamma = \frac{\bar{\delta u}^2}{2} \frac{w^2 u^2 (u - lk_y)^2}{l^6 \tilde{q}^4} \sec^2 \theta. \quad (57)$$

This expression vanishes (remember $u \neq 0$) for $u = lk_y$, which is equivalent to $u = \varepsilon \sin \theta$. Together with the barrier resonance condition, this fixes $\varepsilon_n = n\pi l/w$. Therefore, resonances should occur whenever

$$\tilde{\theta}_n = \arcsin(u/\varepsilon_n) \quad (58)$$

For the parameters of Fig. 5 ($u = 2$, $\varepsilon = 2\pi$, and $w = l/2$), Eq. (58) predicts a resonance at $\tilde{\theta}_1 \approx 18.6^\circ$, in perfect agreement with the data in Fig. 5c. As shown by the data for stronger disorder, the delocalization resonance only holds to lowest order of the weak-disorder expansion.

Are there other delocalization resonances caused by $S' = 0$? A direct answer is difficult on account of the rather complex expression for S' . Numerically, we have scanned the values of S' and find that when S' is zero, the associated solution falls inside a band gap. This being the case, the $S' = 0$ condition does not produce new delocalization resonances, in marked difference to the scalar GSLs studied in Sec. III B 2.

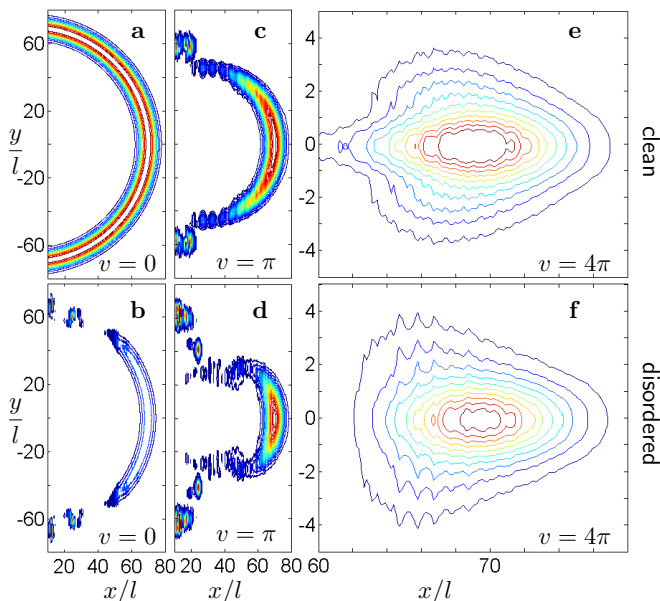


FIG. 6. Contour plot of the probability density, from 2D wave-packet dynamics simulations, for various amplitudes $v = Vl/\hbar v_F$ of clean (upper row) and amplitude-disordered (lower row) scalar GSL potentials $V(x)$, Eq. (2). The time evolution samples all incidence angles θ at once, starting with an isotropic wave packet centered around energy $\varepsilon = El/\hbar v_F = 2\pi$ (see text). Comparison between panels **a-b**, and **c-d** demonstrates disorder-induced filtering: since wave-packet components at larger angle θ have a shorter localization length, they cannot contribute to propagation in x direction, and the transmitted part of the wave packet appears more focused. The GSL potential in panels **e-f** is sufficiently strong to induce the wave-packet collimation that accompanies the emergence of new Dirac cones. Panel **f** shows that disorder has rather little effect on collimation.

V. WAVE PACKET DYNAMICS: DISORDER-INDUCED FILTERING

Our analytical results have revealed an interesting functional dependence of the localization length upon the incident angle of charge carriers. In particular, the Lyapunov exponent $\gamma = l/l_{\text{loc}}$ of a scalar GSL is proportional to $\tan^2 \theta$. This factor indicates a strong angular dependence of disorder-induced localization: the localization length diverges for small θ and quickly decreases as θ increases. Certainly, for θ too close to $\theta = \pi/2$, an infinite Lyapunov exponent or vanishing localization length is an artifact of weak-disorder perturbation theory. With this clarified, it is nevertheless clear that scattering waves with larger θ tend to be much more localized than those with small θ . And wave components with localization length shorter than the GSL sample will not contribute to the conductance. This realizes a filtering effect due to disorder. The main goal of the present, comparatively short section is to confirm this effect by a direct dynamical simulation of wave-packet transmission across a scalar GSL, both with and without disorder.

Figure 6 shows the result of a numerical solution of the time-dependent Dirac equation with Hamiltonian (1) and a scalar GSL potential, Eq. (2), with symmetric barrier width $w = 0.5l$ filling the half-space $x > 10l$. In order to sample all incidence angles at once, we choose as initial condition an isotropic wave packet with momentum components $\Psi(p) \propto \exp\{-(|p| - p_0)^2/(2\Delta p^2)\}$ centered on the radial value $p_0 = 2\pi\hbar/l$ with spread $\Delta p = 0.2\hbar/l$; the wave packet's central energy therefore is $\varepsilon = 2\pi$ in lattice units. In Fig. 6, we plot the probability density at time $t = 70l/v_F$; in some cases, a substantial part of the wave packet is reflected into the half-space $x < 10l$ (not shown). The upper row shows the results for clean GSLs of different strengths, whereas the lower row shows the results for a single realization of the corresponding disordered GSLs with fluctuating potential heights.

Panels **a** and **b** compare a pristine graphene sheet to a purely amplitude-disordered scalar GSL with zero mean potential strength and equiprobable fluctuations $\delta v \in [-1, 1]$. Whereas the clean substrate allows for isotropic propagation, in the disordered GSL the larger-angle components are localized more strongly, as expressed by the $\tan^2 \theta$ -behavior of the Lyapunov exponent, Eq. (43). Consequently, the propagating part of the wave packet is concentrated around the forward direction $\theta = 0$, thus supporting our filtering conjecture above.

Panels **c** and **d** compare again the clean and disordered situation, now in presence of a GSL with finite strength $v = \pi$, with the same lattice geometry and energy as used for Fig. 3, but relatively strong amplitude fluctuations of $\pm 30\%$. A strong filtering effect analogous to panel **b** is observed, where the largest part of the transmitted probability density is concentrated in the forward direction $\theta = 0$, as expressed by the overall $\tan^2 \theta$ -behavior of the Lyapunov exponent, Eq. (40).

The wave propagation in the clean GSL of panel **c** is quite isotropic, because the associated dispersion relation is almost isotropic for the parameters chosen. If, however, the potential strength of a scalar GSL is greater than a certain critical value, new Dirac points emerge.²⁸ The resulting, strongly anisotropic dispersion relation then collimates the wave packet.²³ This is shown in panel **e**, where the potential strength $v = 4\pi$ makes the wave packet stay sharply focused in the forward direction. We have investigated whether this collimation effect is robust against disorder. Panel **f** shows the effect of 10% fluctuations in potential strength. The collimation is seen to survive, with hardly noticeable disorder effects. A quantitative analysis is difficult because the new Dirac points appear at band edges where the weak-disorder expansion we have used fails. Instead, one could possibly adapt the appropriate singular-point expansions^{64,65} to the Dirac-GSL problem, which is a research program beyond the scope of the present work. Here, we conclude that disorder-induced filtering can coexist with band-structure collimation.

VI. CONCLUDING REMARKS

Drawing on a general weak-disorder expansion, we have derived the Lyapunov exponent (inverse localization length) of various 1D disordered GSLs modeled by random delta or rectangular potentials, both for scalar and vector potentials. The analytical results have been thoroughly checked by numerical experiments. We emphasize that, though the GSL is assumed to be 1D, the physics is far more complicated than for a conventional 1D scattering problem due to the intrinsic coupling between the translational motion and the spinor degree of freedom. One important complication we have predicted is the strong dependence of the localization length on the incident angle of the charge carriers injected to a GSL. To our knowledge, this is the first time that a complete theoretical picture of this incident-angle dependence is obtained. We have also proposed to exploit such angular dependence of the localization length to turn disorder into good use, namely, a possible disorder-assisted filtering effect. Considering that large-size GSLs may be manufactured in the near future, our theoretical results offer a quantitative tool to analyze and predict disorder effects in GSLs.

Our analytical and numerical results also provide evidence for intriguing delocalization resonances: Along specific incident angles, the localization exponent can be identically zero, or at least approach zero for weak disorder. Both scalar and vector GSLs admit delocalization resonances in the conduction band, but for opposite reasons: scalar potentials can have an approximate, weak-disorder resonance because a complex term has zero solutions [i.e., $S' = 0$, see Eq. (40) and (41)], whereas vector potentials have an approximate resonance because of a simple barrier resonance condition [$\sin \varphi = 0$, see Eq. (55)]. Moreover, the corresponding δ -limits of scalar and vector GSLs show very distinct features: the scalar δ GSL admits an exact delocalization by virtue of an interpeak resonance, whereas the vector δ GSL has no resonance at all in the conduction band. In all cases, it is important to realize that whenever numerical or laboratory experiments are performed with finite-size samples, a lowest-order vanishing Lyapunov exponent can very well appear as a rather sharp mobility jump, which signals an effective delocalization across the sample.^{67–69}

In the context of 2D GSLs, a recent study⁷⁰ cautioned that lattice constants less than 10 nm may induce inter-valley scattering or sublattice symmetry breaking, either of which may lead to a band gap and hence break the linear dispersion relation of the charge carriers. The implication of this important finding for our work is twofold. First, to directly apply our theoretical results based on a linear dispersion relation, it is safer to consider GSLs with lattice constants larger than 10 nm or with a potential preserving the symmetry between different Dirac points or between different sublattices. Second, as a possible extension of this work, one may now also apply our main theoretical tool here to investigate how a disordered

GSL with a sufficiently small lattice constant may generate a novel physical situation, where charge carriers possess disordered mass as a consequence of inter-valley scattering or sublattice symmetry breaking.

ACKNOWLEDGMENTS

J.G. is grateful to Prof. Chun Zhang for stimulating discussions on graphene superlattices and for providing several useful references on this topic. C.M. acknowledges helpful correspondence with Felix Izrailev.

Appendix A: Details of weak-disorder expansion

This appendix provides some details of the analytical calculation leading to the weak-disorder Lyapunov exponent given by Eq. (22) and Eq. (23).

1. Absence of mixed-fluctuation terms

The starting point is Eq. (21), where $\lambda_{\pm} = e^{\pm i\mu}$, $\mu \in \mathbb{R}$, describes a propagating solution in the clean GSL. A Taylor expansion to quadratic order in the fluctuations ϵ_n leads to

$$\begin{aligned} \frac{1}{2N} \ln |(P_N)_{11}|^2 = & \text{Re} \left\{ \frac{\tilde{M}'_{11}}{\lambda_+} \right\} \frac{1}{N} \sum_{n=1}^N \epsilon_n \quad (\text{A1}) \\ & + \text{Re} \left\{ \frac{\tilde{M}''_{11}}{\lambda_+} - \frac{\tilde{M}'_{11}{}^2}{\lambda_+^2} \right\} \frac{1}{N} \sum_{n=1}^N \frac{\epsilon_n^2}{2} \\ & + \text{Re} \left\{ \tilde{M}'_{12} \tilde{M}'_{21} \frac{1}{N} \sum_{n < m} \lambda_+^{2(n-m)} \epsilon_n \epsilon_m \right\}. \end{aligned}$$

First, we justify that the last line only gives a negligible contribution under the ensemble average. In terms of the complex random variable $z_n = \epsilon_n \lambda_+^{2n} = \epsilon_n e^{2in\mu}$, the double sum rewrites

$$\frac{1}{N} \sum_{n < m} z_n z_m^* = \frac{1}{2N} \left| \sum_{n=1}^N z_n \right|^2 - \frac{1}{2N} \sum_{n=1}^N |z_n|^2 \quad (\text{A2})$$

In the second term, we recognize the variance $\overline{|z|^2} = \overline{\epsilon^2} =: \sigma^2$ in the limit $N \rightarrow \infty$. The whole expression (A2) can be written as $\sigma^2(|y_i|^2 - 1)/2$, where the random variable $y_i \equiv \sum_{n=1}^N z_n^{(i)} / (\sqrt{N}\sigma)$ fluctuates as samples i are drawn from the ensemble. Now, according to the Berry-Esseen theorem, in the limit $N \rightarrow \infty$ the probability distribution of $|y|$ converges to the standard normal distribution, with unit variance $\overline{|y|^2} = 1$. As a consequence, $\sigma^2(\overline{|y|^2} - 1) = 0$, such that the whole expression (A2) gives zero contribution after the ensemble average.

Then, the vanishing fluctuation mean (19) makes also the first line in (A1) vanish. Thus, only the variance (20)

in the second line contributes to

$$\gamma = \lim_{N \rightarrow \infty} \frac{\ln |(P_N)_{11}|^2}{2N} = \frac{\overline{\epsilon^2}}{2} \operatorname{Re} \left\{ \frac{\tilde{M}'_{11}}{\lambda_+} - \frac{(\tilde{M}'_{11})^2}{\lambda_+^2} \right\}, \quad (\text{A3})$$

which is the result stated as Eq. (22).

2. Diagonalization procedure

As the last task, we need to express the matrix elements \tilde{M}'_{11} and \tilde{M}''_{11} of the diagonal representation through the transfer-matrix parameters $\{\alpha, \beta, \phi\}$ as defined in (12). In an intermediate step, we parameterize the transfer matrix as

$$M = \begin{pmatrix} a & b \\ b^* & a^* \end{pmatrix}, \quad (\text{A4})$$

where

$$a = e^{i\alpha} \sec \phi, \quad (\text{A5})$$

$$b = e^{i\beta} \tan \phi, \quad (\text{A6})$$

have to satisfy the constraint $\det M = |a|^2 - |b|^2 = 1$. The diagonal representation $\tilde{M} = \operatorname{diag}(\lambda_+, \lambda_-) = P^{-1}MP$ is attained by a basis transformation with

$$P = \begin{pmatrix} b & b \\ \lambda_+ - a & \lambda_- - a \end{pmatrix}, \quad (\text{A7})$$

$$P^{-1} = \frac{1}{b(\lambda_- - \lambda_+)} \begin{pmatrix} \lambda_- - a & -b \\ -(\lambda_+ - a) & b \end{pmatrix}. \quad (\text{A8})$$

Again, we assume that the eigenvalues $\lambda_{\pm} = e^{\pm i\mu}$ form a complex conjugate ($\mu \in \mathbb{R}$), and non-degenerate ($\mu \neq n\pi$ for all $n \in \mathbb{Z}$) pair since we seek the Lyapunov exponent of inside-conduction-band solutions.

Elementary algebra leads to

$$\tilde{M}'_{11} = (P^{-1}M'P)_{11} = \frac{2\lambda_+ \operatorname{Re}\{a'\}}{\lambda_+ - \lambda_-}, \quad (\text{A9})$$

where the useful identities $\lambda_+ + \lambda_- = a + a^*$ and $(\det M)' = 2\operatorname{Re}\{a^*a' - b^*b'\} = 0$ have been employed. Furthermore, $\operatorname{Re}\{a\} = \cos \mu$ entails $\operatorname{Re}\{a'\} = -\mu' \sin \mu$, and since $\lambda_+ - \lambda_- = 2i \sin \mu$, Eq. (A9) implies

$$-\left(\tilde{M}'_{11}/\lambda_+\right)^2 = \frac{(\operatorname{Re}\{a'\})^2}{\sin^2 \mu} = \mu'^2, \quad (\text{A10})$$

which is the second term needed in Eq. (A3).

Proceeding similarly, one finds for the first term

$$\frac{\tilde{M}''_{11}}{\lambda_+} = \frac{\operatorname{Re}\{a''\}}{i \sin \mu} + \frac{\operatorname{Re}\{a^*a'' - b^*b''\}}{-i \sin \mu} (\cos \mu - i \sin \mu). \quad (\text{A11})$$

We only need its real part,

$$\begin{aligned} \operatorname{Re} \left\{ \lambda_+^{-1} \tilde{M}''_{11} \right\} &= \operatorname{Re}\{a^*a'' - b^*b''\} = |b'|^2 - |a'|^2 \\ &= (\phi'^2 - \alpha'^2) \sec^2 \phi + \beta'^2 \tan^2 \phi. \end{aligned} \quad (\text{A12})$$

Substituting Eq. (A10) and (A12) into Eq. (A3), we have

$$\gamma = \frac{\overline{\epsilon^2}}{2} \left\{ \mu'^2 + (\phi'^2 - \alpha'^2) \sec^2 \phi + \beta'^2 \tan^2 \phi \right\}, \quad (\text{A13})$$

Further algebraic manipulations lead to the identity

$$\mu'^2 + (\phi'^2 - \alpha'^2) \sec^2 \phi = \frac{\tan^4 \phi}{1 - \sec^2 \phi \cos^2 \alpha} \left[\left(\frac{\sin \alpha}{\sin \phi} \right)' \right]^2, \quad (\text{A14})$$

which then results in the final expression Eq. (23) for the weak-disorder Lyapunov exponent.

* phygj@nus.edu.sg

¹ J. C. Slonczewski and P. R. Weiss, Phys. Rev. **109**, 272 (1958).

² G. W. Semenoff, Phys. Rev. Lett. **53**, 2449 (1984).

³ F. D. M. Haldane, Phys. Rev. Lett. **61**, 2015 (1988).

⁴ A. H. Castro Neto, F. Guinea, N. M. R. Peres, K. S. Novoselov, and A. K. Geim, Rev. Mod. Phys. **81**, 109 (2009).

⁵ V. P. Gusynin and S. G. Sharapov, Phys. Rev. B **71**, 125124 (2005).

⁶ M. S. Purewal, Y. Zhang and P. Kim, Phys. Status Solidi B **243**, 3418 (2006).

⁷ O. Klein, Z. Phys. **53**, 157 (1929).

⁸ M. I. Katsnelson, K. S. Novoselov, and A. K. Geim, Nat. Phys. **2**, 620 (2006).

⁹ J. Schliemann, D. Loss, and R. M. Westervelt, Phys. Rev. Lett. **94**, 206801 (2005); W. Zawadzki, Phys. Rev. B **72**, 085217 (2005); R. Winkler, U. Zulicke, and J. Bolte, *ibid.*

75, 205314 (2007).

¹⁰ G. Juzeliunas, J. Ruseckas, M. Lindberg, L. Santos, and P. öhberg, Phys. Rev. A **77**, 011802 (2008).

¹¹ K. L. Lee, B. Grémaud, R. Han, B.-G. Englert, and C. Miniatura, Phys. Rev. A **80**, 043411 (2009).

¹² Q. Zhang, J. B. Gong, and C. H. Oh, Phys. Rev. A **81**, 023608 (2010).

¹³ E. Alba, X. Fernandez-Gonzalvo, J. Mur-Petit, J. J. Garcia-Ripoll, and J. K. Pachos, arXiv:1107.3673v1 (2011).

¹⁴ S. E. Savel'ev and A. S. Alexandrov, arXiv:1103.5983v1 (2011).

¹⁵ L. Lamata, J. Casanova, R. Gerritsma, C. F. Roos, J. J. Garcia-Ripoll, and E. Solano, New J. Phys. **13**, 095003 (2011).

¹⁶ W. Zawadzki and T. M. Rusin, J. Phys.: Condens. Matter **23** (2011) 143201.

¹⁷ R. G. Unanyan, J. Otterbach, and M. Fleischhauer, Phys.

- Rev. Lett. **105**, 173603 (2010).
- ¹⁸ P. W. Anderson, 1958, Phys. Rev. **109**, 1492 (1958).
- ¹⁹ B. Kramer and A. MacKinnon, Rep. Prog. Phys. **56**, 1469 (1993).
- ²⁰ C. Bai, X. Zhang, Phys. Rev. B **76**, 075430 (2007).
- ²¹ C.-H. Park, L. Yang, Y.-W. Son, M. Cohen, S. G. Louie, Nat. Phys. **4**, 213-217 (2008).
- ²² M. Barbier, F. M. Peeters, P. Vasilopoulos, J. J. Milton Pereira, Phys. Rev. B **77**, 115446 (2008).
- ²³ C.-H. Park, Y.-W. Son, L. Yang, M. L. Cohen, S. G. Louie, Nano Lett. **8**, 2920 (2008).
- ²⁴ J. H. Ho, Y. H. Chiu, S. J. Tsai, M. F. Lin, Phys. Rev. B **79**, 115427 (2009).
- ²⁵ L. Brey, H. A. Fertig, Phys. Rev. Lett. **103**, 046809 (2009).
- ²⁶ M. Barbier, P. Vasilopoulos, F. M. Peeters, Phys. Rev. B **81**, 075438 (2010).
- ²⁷ L.-G. Wang and S.-Y. Zhu, Phys. Rev. B **81**, 205444 (2010).
- ²⁸ C.-H. Park, L. Z. Tan, and S. G. Louie, Physica E **43**, 651 (2011).
- ²⁹ M. R. Masir, P. Vasilopoulos, A. Matulis, and F. M. Peeters, Phys. Rev. B **77**, 235443 (2008).
- ³⁰ M. R. Masir, P. Vasilopoulos, and F. M. Peeters, Phys. Rev. B **79**, 035409 (2009).
- ³¹ S. Ghosh and M. Sharma, J. Phys.: Cond. Matt. **21**, 292204 (2009).
- ³² L. Dell'Anna and A. D. Martino, Phys. Rev. B **79**, 045420 (2009).
- ³³ Q.-S. Wu, S.-N. Zhang and S.-J. Yang, J. Phys.: Cond. Matt. **20**, 485210 (2008).
- ³⁴ I. Snyman, Phys. Rev. B **80**, 054303 (2009).
- ³⁵ L. Z. Tan, C.-H. Park, and S. G. Louie, Phys. Rev. B **81**, 195426 (2010).
- ³⁶ S. Gattenlöhner, W. Belzig, and M. Titov, Phys. Rev. B **82**, 155417 (2010).
- ³⁷ A. Isacsson, L. M. Jonsson, J. M. Kinaret, and M. Jonson, Phys. Rev. B **77**, 035423 (2008).
- ³⁸ F. Guinea, M. I. Katsnelson, and M. A. H. Vozmediano, Phys. Rev. B **77**, 075422 (2008).
- ³⁹ T. O. Wehling, A. V. Balatsky, M. I. Katsnelson, and A. I. Lichtenstein, Europhys. Lett. **84**, 17003 (2008).
- ⁴⁰ K. S. Novoselov, A. K. Geim, S. V. Morozov, D. Jiang, Y. Zhang, S. V. Dubonos, I. V. Grigorieva, and A. A. Firsov, Science **306**, 666 (2004).
- ⁴¹ K. S. Novoselov, A. K. Geim, S. V. Morozov, D. Jiang, M. I. Katsnelson, I. V. Grigorieva, S. V. Dubonos, and A. A. Firsov, Nature **438**, 197 (2005).
- ⁴² Y. Zhang, Y. W. Tan, H. L. Stormer, and P. Kim, Nature **438**, 201 (2005).
- ⁴³ J. C. Meyer, C. O. Girit, and M. F. Crommie, A. Zettl, Appl. Phys. Lett. **92**, 123110 (2008).
- ⁴⁴ S. Marchini, S. Günther, and J. Wintterlin, Phys. Rev. B **76**, 075429 (2007).
- ⁴⁵ A. L. Vazquez de Parga, F. Calleja, B. Borca, M. C. G. P. Jr, J. J. Hinarejo, F. Guinea, and R. Miranda, Phys. Rev. Lett. **100**, 056807 (2008).
- ⁴⁶ P. W. Sutter, J.-I. Flege, and E. A. Sutter, Nature Mater. **7**, 406 (2008).
- ⁴⁷ D. Martoccia, P. R. Willmott, T. Brugger, M. Björck, S. Günther, C. M. Schlepütz, A. Cervellino, S. A. Pauli, B. D. Patterson, S. Marchini, J. Wintterlin, W. Moritz, and T. Greber, Phys. Rev. Lett. **101**, 126102 (2008).
- ⁴⁸ J. Coraux, A. T. N'Diaye, C. Busse, and T. Michely, Nano Lett. **8**, 565 (2008).
- ⁴⁹ A. T. N'Diaye, J. Coraux, T. N. Plasa, C. Busse, and T. Michely, New J. Phys. **10**, 043033 (2008).
- ⁵⁰ I. Pletikosić, M. Kralj, P. Pervan, R. Brako, J. Coraux, A. T. N'Diaye, C. Busse, and T. Michely, Phys. Rev. Lett. **102**, 056808 (2009).
- ⁵¹ A. Avsar *et al.*, Nano Lett. **11**, 2363 (2011).
- ⁵² A. De Martino, L. Dell'Anna, and R. Egger, Phys. Rev. Lett. **98**, 066802 (2007).
- ⁵³ V. M. Pereira and A. H. Castro Neto, Phys. Rev. Lett. **103**, 046801 (2009).
- ⁵⁴ M. R. Masir, P. Vasilopoulos, and F. M. Peeters, New J. Phys. **11**, 095009 (2009).
- ⁵⁵ S.-L. Zhu, D.-W. Zhang, and Z. D. Wang, Phys. Rev. Lett. **102**, 210403 (2009).
- ⁵⁶ Y. P. Bliokh, V. Freilikher, S. Savel'ev, and F. Nori, Phys. Rev. B **79**, 075123 (2009).
- ⁵⁷ P. Markoš and C. M. Soukoulis, *Wave Propagation: from electrons to photonic crystals and left-handed materials* (Princeton University Press, Princeton and Oxford, 2008), Chap. 1-4.
- ⁵⁸ C. A. Müller and D. Delande, chap. 9 in C. Miniatura *et al.* (eds), *Les Houches 2009 - Session XCI: Ultracold Gases and Quantum Information* (Oxford University Press, Oxford 2011); arXiv:1005.0915
- ⁵⁹ A. Galindo, P. Pascual, *Quantum Mechanics I* (Springer, Berlin, 1990).
- ⁶⁰ H. Furstenberg and H. Kesten, Ann. Math. Statist. **31**, 457 (1960); H. Furstenberg, Trans. Amer. Math. Soc. **108**, 377 (1963).
- ⁶¹ A. A. Abrikosov, Sol. State Comm. **37**, 997 (1981).
- ⁶² M. V. Berry and S. Klein, Eur. J. Phys. **18**, 222 (1997).
- ⁶³ B. Derrida, K. Mecheri, and J. Pichard, J. Phys. France **48**, 733 (1987).
- ⁶⁴ B. Derrida, E. Gardner, and J. Physique **45** 1283 (1984).
- ⁶⁵ F. M. Izrailev, S. Ruffo, and L. Tessieri, J. Phys. A: Math. Gen. **31**, 5263 (1998).
- ⁶⁶ M. Barbier, P. Vasilopoulos, and F. M. Peeters, Phys. Rev. B **80**, 205415 (2009).
- ⁶⁷ F. M. Izrailev, A. A. Krokhin, S. E. Ulloa, Phys. Rev. B **63**, 041102 (2001).
- ⁶⁸ A. Krokhin, and F. M. Izrailev, U. Kuhl, H.-J. Stöckmann, S. E. Ulloa, Physica E **13**, 695 (2002).
- ⁶⁹ P. Lugan, A. Aspect, L. Sanchez-Palencia, D. Delande, B. Grémaud, C. A. Müller, C. Miniatura, Phys. Rev. A **80**, 023605 (2009).
- ⁷⁰ A. Zhang, Z. Dai, L. Shi, Y. P. Feng, and C. Zhang, J. Chem. Phys. **133**, 224705 (2010).